*Bangladesh Journal of Physics, Vol. **33**, Issue 1, pp. 1 – 13, June 2026*

FIRST PRINCIPLE STUDY VIA ASR TO OBSERVE THE RELATIVISTIC EFFECTS IN Fe_XPt_{1-X} DISORDERED ALLOYS

M. M. RAHMAN[1*], M. M. ISLAM[2], F. ALAM[3], A. HUDA[1]

[1]*Department of Physics, Jagannath University, Dhaka-1100, Bangladesh*
[2]*Department of Computer Science and Engineering, Central Women's University, Dhaka, Bangladesh*
[3]*Department of Physical Sciences, Independent University Bangladesh (IUB), Dhaka-1229, Bangladesh*
Corresponding author email: majidurrahman@phy.jnu.ac.bd

Received on 13.01.2026, Revised received on 02.05.2026, Accepted for publication on 04.05.2026

DOI: *https://doi.org/10.3329/bjphy.v33i1.87148*

ABSTRACT

Fe_xPt_{1-x} alloys are promising for spintronic applications, particularly in cases involving relativistic effects and electric and magnetic properties, arising from spin-orbit coupling (SOC). It is very difficult to study the relationship between atomic disorder and relativistic effects in any computational model. Usually, the Coherent Potential Approximation (CPA) is used as a mean field method, with limitations for extreme disorder variations, and it presents material properties. In this task, two methods are combined: The Augmented Space Recursion (ASR) approximation and another first-principles methodology (DFT). The outcome of our research shows that SOC significantly revises the density of states (DOS) in Fe_xPt_{1-x} alloys, leading to dramatic changes in their electronic and magnetic properties. This property also plays a vital role in relativistic phenomena in alloys. For disordered alloy systems, this investigation aims to provide a clear understanding of the relativistic effects and their electric and magnetic properties of Fe_xPt_{1-x} alloys.

Keywords: *DFT, FePt alloys, ASR, Band energy, DOS*

1. INTRODUCTION

In the modern age, transition metal alloys have enormous applications in technological fields. These materials are used in various fields, such as high-density magnetic storage [1], cutting-edge magnetic sensors [2,3], magneto-optical recording [4–6], and catalytic systems [7]. Disordered Fe_xPt_{1-x} alloys are of significant interest due to their outstanding structural, electronic, and magnetic properties. These properties are cruical for modern industrial and technological applications. Relativistic effects, arising from SOC and scalar relativistic interactions of the heavy Fe and Pt atoms, are significant in disordered Fe_xPt_{1-x} alloys and strongly influence their electronic structure, magnetism, and stability. These relativistic effects have a significant impact on applications in data storage and spintronic devices. Many researchers have used the CPA to investigate various properties of disordered alloys [8]. However, the CPA is not sufficiently accurate method for describing complex electronic interactions and short-range order. In ref. [9], density functional theory (DFT) works well for ordered systems; however, disordered systems are also described using parameters derived from order system. These drawbacks are particularly impact for relativistic and disorder related phenomena. These limitations overcome using the Augmented Space Recursion (ASR) method [10], which is a potential alternative for treating configuration-dependent interactions and disorder in alloys. For

Fe_xPt_{1-x} alloys, the ASR approximation enables the observation of relativistic effects in higher-order electronic correlations. On the other hand, CPA is used to calculate the average properties in Fe_xPt_{1-x} alloys. The application of the ASR potential is not yet well established for disorder alloys. Understanding how relativistic effects influence fundamental properties such as mechanical, magnetic, and thermal stability is important for modern technologies. Fe_xPt_{1-x} alloys are used in devices for magnetic data storage, spintronics, catalysis, and related applications. For the validation of theoretical computations, good agreement with experimental data is required to establish new computational models. Disordered Fe_xPt_{1-x} alloys make a major contribution to the development of advanced data storage devices, which have emerged in the field of quantum computing and viable energy technologies.

2. METHODOLOGY

2.1. Methodology of Spin-Orbit Coupling for Ordered and Disordered Alloys

Relativistic effects are a crucial factor in conventional electronic structure calculations of alloys containing heavy elements. The choice of computational approaches and associated approximations for alloys containing heavy elements has a critical impact on the final assessment of their stability. Most previous studies on alloys incorporated only scalar relativistic corrections. Here, we introduce a methodology that also accounts for spin-orbit coupling.

2.2 Spin-orbit Coupling in Ordered Systems

Let us use a basis set to represent the Hamiltonian: the muffin-tin orbitals obtained from solutions of the Schrödinger equation with scalar relativistic terms, but without the spin-orbit correction. The appropriateness or otherwise of the basis set will be clear from the systems under study. For this basis, the Hamiltonian is presented by;

$$\underline{H} = \underline{E_{\nu}} + \underline{h}^{\beta} - \underline{h}^{\beta}\,\underline{o}\,\underline{h}^{\beta} + \underline{H_{SO}} \tag{1}$$

here,
$$h^{\beta}_{RL,R'L'} = \left[C^{\beta}_{RL} - E_{\nu l} + \Delta^{\beta\ 1/2}_{RL} S^{\beta}_{RL,RL} \Delta^{\beta\ 1/2}_{RL}\right]\delta_{R,R'}\delta_{L,L'} +$$

$$\ldots + \left[\Delta^{\beta\ 1/2}_{RL} S^{\beta}_{RL,R'L'} \Delta^{\beta\ 1/2}_{R'L'}\right](1 - \delta_{RR'}) \tag{2}$$

The potential parameters C^{β}_{RL} and $\Delta^{\beta\ 1/2}_{RL}$ are obtained self-consistently from LSDA-based TB-LMTO-ASR calculation. $S^{\beta}_{RL,R'L'}$ is the structure matrix of the TB-LMTO formalism.

Here, L denotes the composite index $\{l, m, m_s\}$ including the spin-index. Finally, the matrix elements of the spin-orbit term are

$$H^{SO}_{RL,R'L'} = A_{R,L,L'} + h^{\gamma}_{RL,RL} B_{R,L,L'} + \hat{B}_{R,L,L'} h^{\gamma}_{RL',RL'} + \cdots$$

$$+ h^{\gamma}_{RL,RL} C_{R,L,L'} h^{\gamma}_{RL',RL'} + \sum_{R'\neq R} \sum_{L_1 L_2} h^{\gamma}_{RL,R'L_1} C_{R'L_1,L_2}\, h^{\gamma}_{R'L_2,RL} \tag{3}$$

$$H^{SO}_{RL,R'L'} = \sum_{L''} \left\{h^{\gamma}_{RL,R''L''} B_{R',L'',L'} + \hat{B}_{R',L,L''} h^{\gamma}_{RL'',R'L'}\right\} + \cdots$$

$$\ldots + \sum_{R''\neq R} \sum_{L_1 L_2} h^{\gamma}_{RL,R''L_1} C_{R'',L_1,L_2}\, h^{\gamma}_{R''L_2,R'L'} \tag{4}$$

The equations (1), (3), and (4) are the representation of the Hamiltonian. For most lattice structures, the tight-binding matrix $\underline{h}^{\beta}$ is short ranged and typically includes interactions only up to nearest neighbor sites. A simple and consistent approximation is to substitute $\underline{h}^{\gamma}$ by $\underline{h}^{\beta}$. The spin-orbit contribution also extends to the 2nd-nearest neighbors. Equation (3) is an ideal for the recursion method. At this point, assuming the *L-S* coupling is weak, many researchers have evaluated its effect on the spectrum of solids using a second-order perturbation theory. However, by obtaining a sparse representation of the Hamiltonian is an appropriate basis, the spectrum can be efficiently determined using the recursion method of Haydock [11][12]. For this, the Hamiltonian operator of our basis is represented by

$$\mathbf{H} = \mathbf{H'} - (\mathbf{H'} - \mathbf{E})\,\mathbf{o}\,(\mathbf{H'} - \mathbf{E}) + \mathbf{H}_{SO} \tag{5}$$

Where,

$$\mathbf{H'} = \sum_{\mathrm{R}} \left[\left\{ C_{RL}^{\beta} + \Delta_{RL}^{\beta\ 1/2} S_{RL,RL}^{\beta} \Delta_{RL}^{\beta\ 1/2} \right\} \delta_{LL'} \right] \mathbf{p}_R + \cdots$$

$$\ldots + \sum_{R \neq R'} \left[\Delta_{RL}^{\beta\ 1/2} S_{RL,R'L'}^{\beta} \Delta_{R'L'}^{\beta\ 1/2} \right] \mathbf{T}_{RR'}$$

$$\mathbf{H}_{SO} = \sum_R H_{RL,RL'}^{SO}\, \mathbf{p}_R + \sum_{R \neq R'} H_{RL,R'L'}^{SO}\, \mathbf{T}_{RR'}$$

$$\boldsymbol{E} = \sum_R E_{\nu L} \delta_{LL'}\, \mathbf{p}_R$$

$$\mathbf{o} = \sum_R o_{RL} \delta_{LL'} \mathbf{p}_R \quad \text{(O is the overlapping matrix)} \tag{6}$$

$\mathbf{T}_{RR'} = |R\rangle\langle R'|$ and $\mathbf{p}_R = |R\rangle\langle R|$ are transfer operators and projections in the Hilbert space *H* spanned by the TB-LMTO basis.

We also defined the O mean overlapping matrix mentioned in equation (5) in the updated manuscript. The input parameters of Augmented Space Recursion are obtained from the computation of the Linearized Muffin Tin Orbital method (TB-LMTO). TB-LMTO (Tight-Binding Linear Muffin-Tin Orbitals) is a specialized, computationally efficient method used to solve the Kohn-Sham equations within the framework of Density Functional Theory (DFT). While DFT provides the theoretical foundation for calculating electronic structures, TB-LMTO serves as a particularly efficient, "first-principles" numerical technique to implement it, especially for complex or large unit-cell solid-state systems. We used our self-developed code for Augmented Space Recursion, where the input parameters are obtained from the LMTO software.

2.3 Spin-orbit Coupling in Disordered Systems

The formulation of 'Spin-orbit Coupling in ordered systems and Surfaces' can be generalized to be applicable for the disordered alloys through the Augmented Space Technique [10]. It was observed that spin-orbit coupling plays a significant role in alloys of heavier elements [13]. The Augmented Hamiltonian acts as an operator in a space which is the product of the space spanned by the countable basis and the space spanned by the configurations of the random variables. The configurational averages are therefore expressed as matrix elements of a specific configuration state, which, by analogy with many-body scattering theory, is referred to as the vacuum state. The configuration-averaged Green's function can then be determined using the recursion method applied to the complete augmented space. The Hamiltonian is written as follows:

$$H \;=\; \Delta^{1/2}[\,\tilde{C} + S - \,(C' + S)o'(C' + S) + \cdots$$

$$\ldots + A' + (C' + S)B' + \hat{B}''(C' + S) + C'\mathcal{C}'C' + S\,C'S]\Delta^{1/2}$$
$$= \Delta^{1/2}\left[\tilde{C} + S - H'\right]\Delta^{1/2} \tag{7}$$

Where we have: $o' = o\,\Delta \qquad \tilde{C} = \frac{C}{\Delta} \qquad C' = \frac{C-E}{\Delta}$

$$\mathcal{C}' = \Delta^{1/2}\mathcal{C}\,\Delta^{1/2} \qquad B' = \Delta^{1/2}B\,\Delta^{-1/2} \qquad B'' = \Delta^{-1/2}B\Delta^{1/2}$$
$$A' = \Delta^{-1/2}A\,\Delta^{-1/2} \tag{8}$$

For a substitutional binary random alloy, the site labelled potential parameters have a binary distribution: taking values appropriate for the A and B constituents with probabilities proportional to their concentrations: x_A and x_B. The corresponding configuration space is isomorphic to that for an Ising model, and the operator whose spectrum is the probability density is:

$$\boldsymbol{M}^R = x_A\boldsymbol{P}_\uparrow + x_B\boldsymbol{P}_\downarrow^R + \sqrt{x_A x_B}\ (\boldsymbol{T}_{\uparrow\downarrow}^R + \boldsymbol{T}_{\downarrow\uparrow}^R) \tag{9}$$

From equation (7) we get:

$$\boldsymbol{G}(z) = \left(z\,\boldsymbol{I} - \Delta^{1/2}\left[\tilde{C} + S - H'\right]\Delta^{1/2}\right)^{-1}$$
$$= \Delta^{-1/2}\left(z\,\Delta^{-1} - \tilde{C} - S + H'\right)^{-1}\Delta^{-1/2} \tag{10}$$

We can now apply the augmented space theorem to derive the following: for any single-site random Hamiltonian element $\boldsymbol{K} \in \mathcal{H}$, the augmentation transformation yields

$$\hat{K} = \sum_R \left\{ \frac{A(K_R)}{A\left(\Delta_R^{-1/2}\right)^2}\boldsymbol{P}_R \otimes \boldsymbol{I} + \frac{B(K_R)}{A\left(\Delta_R^{-1/2}\right)^2}\boldsymbol{P}_R \otimes \boldsymbol{P}_\downarrow^R + \ldots + \frac{F(K_R)}{A\left(\Delta_R^{-1/2}\right)^2}\boldsymbol{P}_R \otimes (\boldsymbol{T}_{\uparrow\downarrow}^R + \boldsymbol{T}_{\downarrow\uparrow}^R) \right\} \tag{11}$$

If we neglect size difference effects, we have, for example,

$$\hat{S} = \sum_R \sum_{R' \neq R} S_{R\,R'}\boldsymbol{T}_{RR'} \otimes \boldsymbol{I}$$

where, K_R and $S_{RR'}$ are matrices $K_{R,LL'}$ and $S_{RL,R'L'}$ in angular momentum-spin indices and,

$$A(K_R) = x_A K_A + x_B K_B,\ B(K_R) = (x_B - x_A)(K_B - K_A),\ F(K_R) = \sqrt{x_A x_B}\ (K_B - K_A)$$

The configuration-averaged Green-function matrix element is:

$$\ll G_{RR}(z) \gg = \ll 1 \left| \left(z\,\hat{I} - \hat{H}_{eff}\right)^{-1} \right| 1 \gg \tag{12}$$

where, $|1\gg = |R \otimes \{\emptyset\}> + \frac{F\left(\Delta_R^{-1/2}\right)}{A\left(\Delta_R^{-1/2}\right)}\ |R \otimes \{R\}\rangle$

and, $\hat{H}_{eff} = [\,z\left(\hat{I} - \hat{\Delta}^{-1}\right) + \hat{\tilde{C}} + \hat{S} - \left(\hat{C}' + \hat{S}\right)\hat{o}'\left(\hat{C}' + \hat{S}\right) + \cdots$

$$\ldots + \hat{A}' + \left(\hat{C}' + \hat{S}\right)\hat{B}' + \hat{B}''\left(\hat{C}' + \hat{S}\right) + \hat{C}'\hat{C}'\hat{C}' + \hat{S}\hat{C}'\hat{S}\,] \tag{13}$$

In the configuration space, states are uniquely identified by the cardinality sequence $\{R_1, R_2, \ldots\}$ indicating the sites where a configuration fluctuation (represented by ↓) occurs relative to the average state (represented by ↑). The configuration-averaged Green's function is then calculated directly through recursion in the augmented space, using $|1\rangle\rangle$ as the initial state. From these averaged Green's

functions, one can subsequently determine the averaged density of states as well as both the local and overall magnetic moments. The recursion method then carries out a change of basis starting from a chosen state in the Hilbert space, repeatedly operating on it by the Hamiltonian and subtracting projection on the earlier members through a three-term recurrence relation [11,12]. In the new basis, the Hamiltonian is tridiagonal, and the Green function is obtained as a continued fraction:

$$G_{RL,RL}(E) = \langle R,L|(E\mathbf{I}-\mathbf{H})^{-1}|R,L\rangle = \cfrac{1}{E-\alpha_1-\cfrac{\beta_1^2}{E-\alpha_2-\cfrac{\beta_2^2}{\ddots\cfrac{\beta_{N-1}^2}{E-\alpha_N-T(E)}}}} \tag{14}$$

$T(E)$ is the appropriate terminator obtained from the initial part of the continued fraction. The terminator preserves the Herglotz analytic properties of the approximated Green function. The above form ensures that the first 2N moments of the density of states are exactly reproduced, and the terminator ensures that the very large moments are also accurately taken into account. We have used the terminator [14]. To obtain the magnetic moment, we first obtain the spheroidized local charge density within an atomic sphere centered at R**.**

3. RESULTS AND DISCUSSION

3.1 The Computational Framework

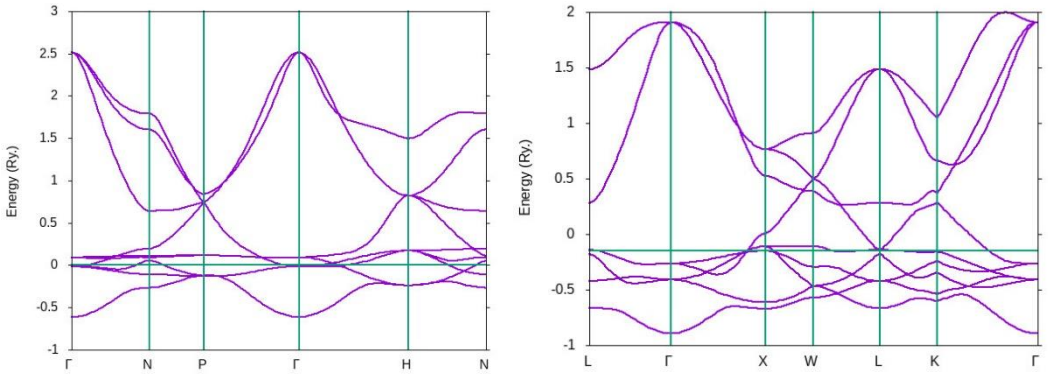

Fig. 1: The band structure of Fe (left) and Pt (right).

The integration of relativistic density functional theory (DFT) with the augmented space recursion (ASR) method is used to study disordered Fe_xPt_{1-x} alloys. The computational framework is used for both disordered alloy systems and relativistic cases. This computational method aims to correctly account for the effects of relativistic interactions in heavy Pt atoms and disordered alloy systems. The computational method is more efficient for observing complex behavior in both relativistic and disordered cases of Fe_xPt_{1-x} alloys. The tight-binding linearized Muffin Tin Orbital (TB-LMTO) method is used to evaluate ordered Fe ferromagnetic and Pt paramagnetic elements, respectively.

We also investigate the electronic structure of the Fe_xPt_{1-x} alloy using the SOC method. For the cubic body-centered Fe and face-centered Pt structures, the lattice parameter was taken as 2.87 Å and 2.79 Å, respectively. Figure 1 illustrates the band structures of Fe and Pt, where the overlap between the valence and conduction bands confirms their metallic characteristics. In contrast, Pt crystallizes in a face-centered cubic (fcc) structure and exhibits a highly symmetric band structure at high symmetry points Γ(G), X, W, and L. The increased band energy upon including SOC is discussed in terms of lowering occupied states and destabilization of unoccupied states due to SOC perturbation are discussed in the work of reference [13].

We use Haydock's recursion method for this study. In this work, the recursion coefficients were computed for 35 pairs over 25 shells of atoms using the Luchini and Nex [14] terminator. The DOS generated by both models was compared to validate the accuracy of our recursion calculations. Figure 2 shows the density of states computed using the LMTO and recursion methods for ferromagnetic Fe (Fig. 2 (a)) and paramagnetic Pt (Fig. 2 (b)), respectively, with the vertical line indicating the Fermi level. In Fe and Pt, the dominant contribution near the Fermi level originates from the d-orbital electrons. The DOS is the mean difference of DOS between the two methods over the energy window around (0.15-0.1) Ryd for both Pt and Fe. For Fe, the mean absolute deviation is (1-1.5) States per/atom/spin, and for Pt it is (0.5-0.6) states per/atom/spin, indicating very good agreement.

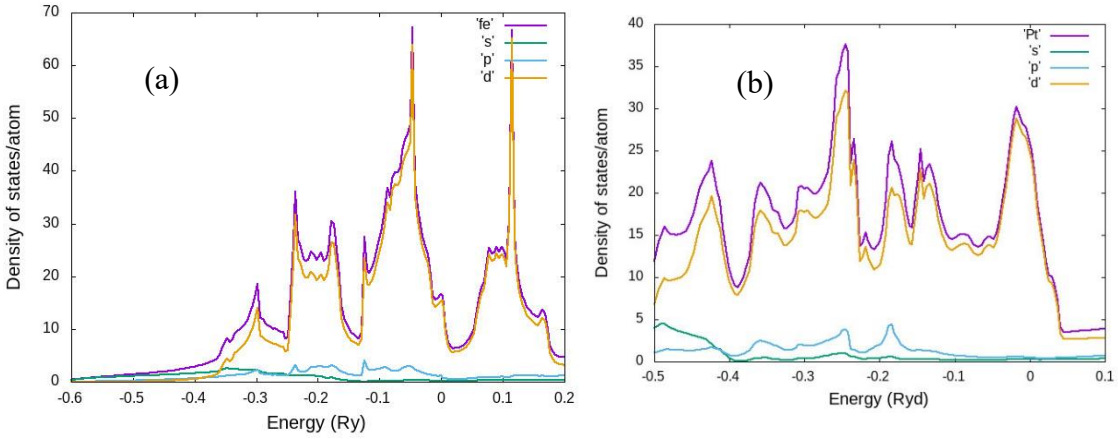

Fig. 2: Density of States of Fe and Pt using LMTO and recursion method.

In the Fig. 2(a), the density of states of Fe for both up and down states are presented. The dark green (up) and magenta(down) is computed from LMTO and in the Fig. 2(b) the density of states of Pt is the green is LMTO.

3.2 Determination of Spin-Orbit Coupling Parameters

The spin–orbit coupling parameters were evaluated using the TB-LMTO method, which applies only to ordered Fe, $FePt_3$, FePt, Fe_3Pt, and Pt. For this purpose, the following crystal parameters were used to obtain the density of states and related data for $FePt_3$, FePt, and Fe_3Pt, as listed in Table 1.

Table 1. The basic data of FePt ordered alloys used in this computation for different Fe and Pt positions.

Alloys	Space-Group	Crystal structure	Lattice parameter (Å)	Atom position
$FePt_3$	Pm3m	Cubic	*a*=*b*=*c*=3.89	1a, Fe=0,0,0, 3c, Pt= 0.5, 0.5, 0
FePt		Tetragonal	*a* =2.73, *b*=2.73, and *c*=3.74	1a, Fe=0,0,0 and 1b, Pt=0.5, 0.5,0
Fe_3Pt	Pm3m	Cubic	*a*=*b*=*c*=3.75	1a, Pt=0,0,0 and 3c, Fe= 0.5, 0.5,0

These data were used in the Newton central difference interpolation formula to obtain the data of Fe_xPt_{1-x} alloys (with x = 0.10 to x=0.90). The evaluated data A_{dd} value for the ordered structures are compared with Huda et. al. [13], and the results are summarized in Table 2.

Table 2. Computed Spin-orbit parameters data and comparison with literature.

Material	Our calculation		Huda et. al. calculation [13]	
	$A_{dd}\uparrow$	$A_{dd}\downarrow$	$A_{dd}\uparrow$	$A_{dd}\downarrow$
Fe	6.22	6.01		
Fe in $FePt_3$	6.05	5.98		
Pt in $FePt_3$	14.03	13.97		
Fe in FePt	6.02	5.85		
Pt in FePt	14.12	14.00		
Fe in Fe_3Pt	6.08	5.99		
Pt in Fe_3Pt	14.10	13.96		
Pt	13.96	13.96	13.97	13.97

The spin–orbit coupling parameter for pure Pt is in good agreement with the values reported by Huda et. al. [13]. We computed the effect of spin–orbit coupling for the disordered system Fe_xPt_{1-x}, with x ranging from 0.1 to 0.9. Only four sets of spin–orbit data are presented in Table 1, the following equations are used to determine the spin–orbit coupling parameters.

$$A_{dd}\uparrow(Pt) = 0.53x^3 + 0.395x^2 + 0.15625x + 14.0796875$$

$$A_{dd}\uparrow(Fe) = -0.11x^3 + 0.885x^2 + 0.735625x + 6.1803125$$

We observed that the line obtained from the above equation completely matches the data presented in Table 2. Figure 3, shows the computed spin–orbit coupling parameters obtained using Newton's interpolation formula.

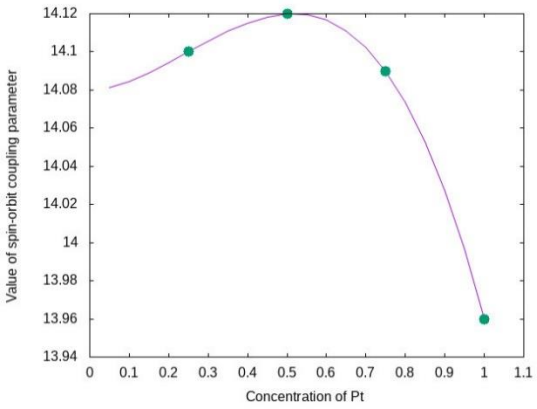

Fig. 3: The estimated value of spin-order coupling parameter $A_{dd} \uparrow (Pt)$ obtained from Newton's interpolation formula. In the similar fashion, all other parameters were computed.

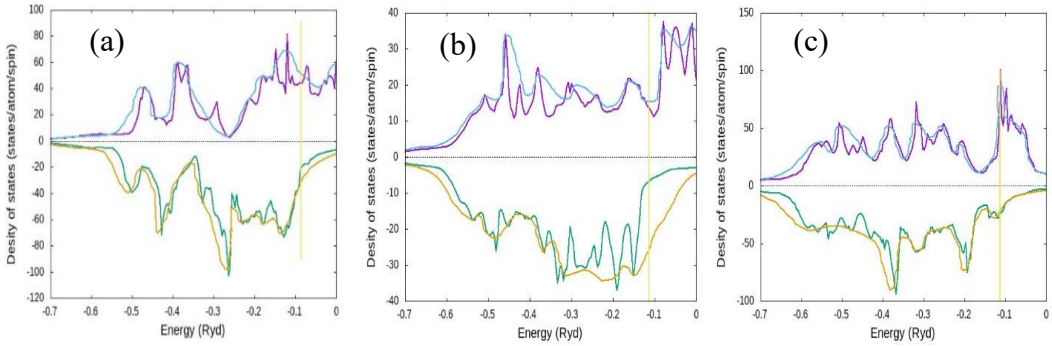

Fig. 4: The density states computed from LMTO and recursion method for Fe_3Pt (a), FePt (b) and $FePt_3$ (c). The vertical line represents the fermi surface. In all cases, magenta and green are LMTO.

The density of states obtained from both the LMTO and recursion methods for ordered (a) Fe_3Pt, (b) FePt and (c) $FePt_3$ is presented in Figure 4. There is good agreement between the density of states results for FePt and $FePt_3$ within the limitations of the available computational facilities. We explicitly note that discrepancies arise from different basis sets. We may also emphasize that the overall spectral features, peak position, bandwidths, and shape near the Fermi level are faithfully reproduced, confirming that the recursion method, when combined with Luchini-Nex terminator, provides a real-space alternative for disordered alloys. The spin–orbit coupling was introduced in the computation, and the densities of states with and without spin orbit coupling for ordered Fe_3Pt, FePt, and $FePt_3$ are shown in Figure 5. The figure indicates that the difference becomes more pronounced as the Pt concentration increases.

The density of states for one spin is shifted to right, while the other is shifted to the left, indicating that the magnetic moment is triggered by spin-orbit coupling. The Change of electronics and magnetics properties is explained elaborately discussed in detail in the below.

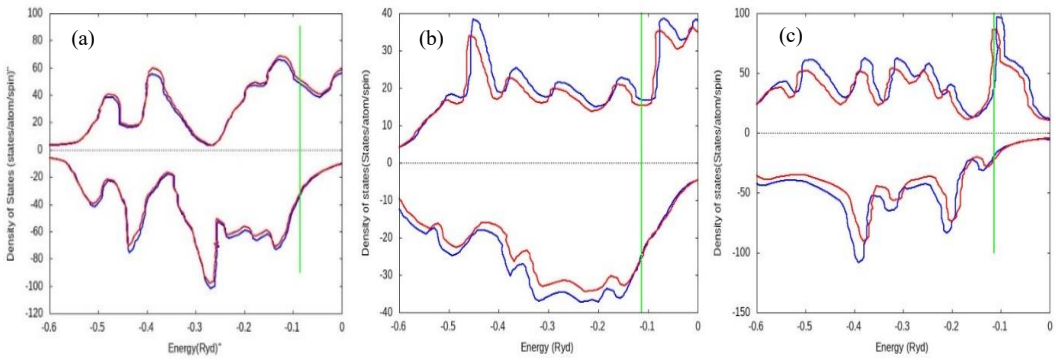

Fig. 5: The density of states of Fe_3Pt (a), FePt (b) and $FePt_3$ (c). The red line is without relativistic correction and blue line is with the relativistic correction. The green line denotes the fermi surface.

Table 3. Electronic energy (Ryd), magnetic moment (Bohr magneton/atom-cell) and density of states at Fermi energy for different ordered metals and alloys used in the study. a) Recursion without LS coupling and b) Recursion with LS coupling.

Examined property	Fe	Fe_3Pt	FePt	$FePt_3$	Pt
Electronic energy (a)	3.299	4.190	4.246	4.731	5.448
Electronic energy (b)	3.310	4.302	4.266	4.851	5.646
Difference (b-a)	0.011	0.112	0.020	0.120	0.198
Magnetic property (a)	2.242	1.883	1.551	1.020	0.000
Magnetic property (b)	2.253	2.084	1.648	1.032	0.038
Difference (b-a)	0.011	0.201	0.097	0.012	0.038

Table 3, presents the effect of including spin–orbit coupling on the magnetic moment and band energy for the ordered Fe_3Pt, FePt, and $FePt_3$ compounds. SOC leads to the degeneracy between different states, and orbital magnetic moments that are not present in the scalar relativistic treatment for Pt, which is a strong SOC due to the high atomic number. This orbital contribution enhances the total magnetic moments. We now include the calculation of orbital magnetic moments (e.g. for FePt, orbital magnetic moment increases from 0.097 μB upon including SOC) and discuss how they align with the spin moment to increase the total magnetization. The required spin-orbit coupling parameters were computed using the equation proposed in the previous. The spin-orbit coupling parameter for pure Pt is in good agreement with the data produced by Huda et. al [13]. For the calculation of the components of the projected and averaged density of states of the binary model for the ferromagnetic and paramagnetic cases, a real-space cluster of 400 atoms and an augmented space shell extending to the sixth nearest neighbor from the starting state were generated and used to compute of eight pairs of recursion coefficients exactly. An analytic terminator proposed by Luchini and Nex was used. The Convergence tests suggested by the authors were carried out to a prescribed accuracy. Using the above procedure, the density of states of Fe_xPt_{1-x} was calculated for x values ranging from 0.1 to 0.9 in increments of 0.1. Using the spin-orbit coupling parameters described in Fig. 6, the methodology of Huda et. al. [13] was used to introduce the spin-orbit coupling in our calculation into the above-mentioned disordered data. The density of states of both with and

without spin-orbit coupling is presented in Fig. 7 (a). We observed that with increasing Pt concentration of the alloy, one of the spins is shifted to the right and another to the left, which decreases the overlap between up and down spin densities of states as a result, the magnetic moment increases.

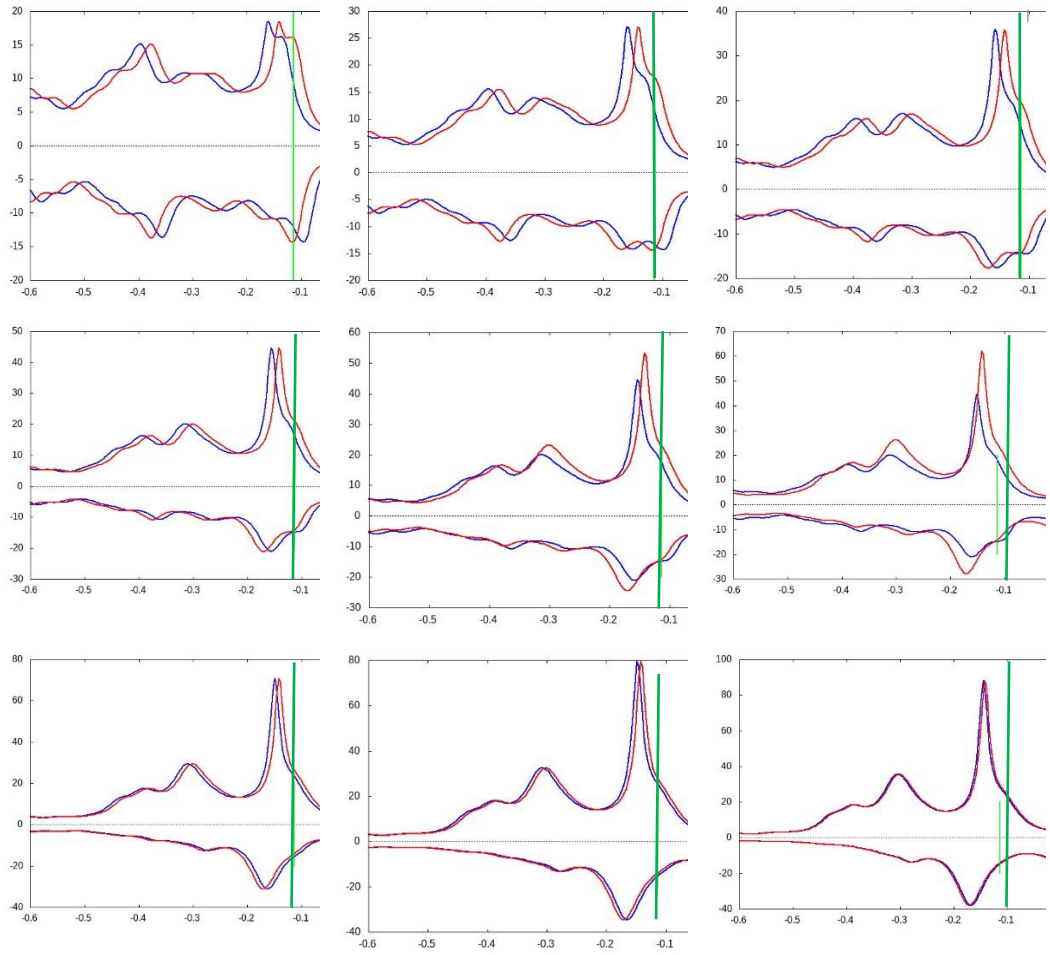

Fig. 6: Comparison of density of states of Fe_xPt_{1-x} (for x=0.10, 0.20, 0.30, 0.40, 0.50, 0.60, 0.70, 0.80, 0.90) without and with relativistic corrections. The red data represent the density of states without spin-orbit coupling, and the blue data represent with spin-orbit coupling. Green line is the Fermi energy. Energy in Rydberg is plotted in the x-axis and density of states (states/atom/spin) is plotted in the y-axis.

Figure 7 (a) shows that including SOC leads to an increase in band energy. The increase in band energy with increasing Pt concentration indicates the SOC effect is stronger in Pt-rich compositions. This behavior is expected because Pt is a heavier element with strong SOC. Figure 7(b), shows that the magnetic moment follows a similar trend to the band energy that is as the Pt concentration increases, the magnetic moment also increases when SOC is considered. This result suggests that

SOC enhances spin polarization or modifies the hybridization in a way that strengthens the magnetic moment. The observation aligns with the fact that heavier atoms like Pt experience stronger SOC effects, influencing both the electronic structure (band energy) and the magnetic properties (magnetic moment). The recursion method used in this study captures this enhancement in both properties due to SOC.

The SOC modifies the Fe 3d and Pt 5d hybridization. If the Pt-rich alloys, the Pt 5d state is more strongly affected, leading to a redistribution of states in the energy window near the Fermi level. We now present the partial DOS for Fe 3d and Pt 5d separately in Fig.6 to show that SOC causes a depletion of Pt 5d state at the Fermi level and a corresponding increase in spin polarization. This reduces the exchange-split DOS overlap between majority and minority spins, which directly explains the rise in magnetic moments. The increased band energy upon including SOC is discussed in terms of lowering occupied states and destabilization of unoccupied states due to SOC perturbation are discussed in the work of reference [13].

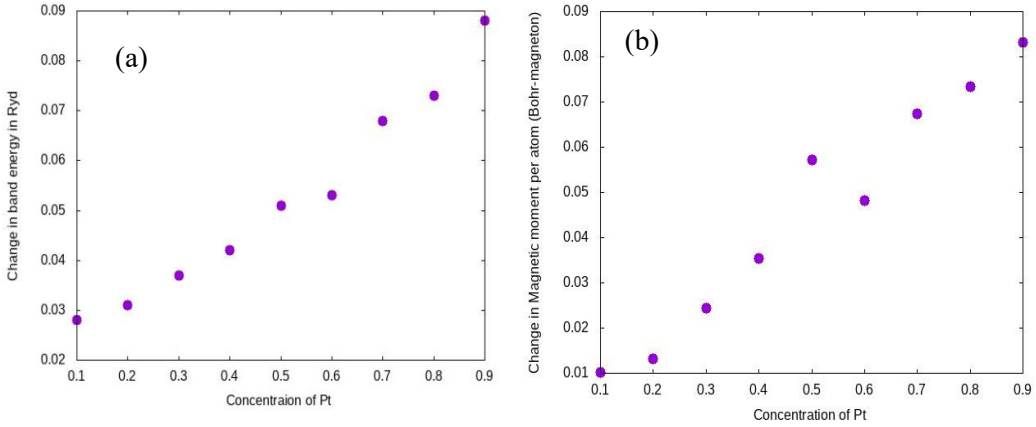

Fig. 7: (a) The change of band energy with and without Spin-Orbit Coupling (SOC), (b) Shows changes in magnetic moments with SOC inclusion.

4. CONCLUSIONS

This study investigates the effects of SOC on the electronic structure and magnetism of disordered Fe_xPt_{1-x} alloys using the ASR method. Independent calculations for ferromagnetic ordered Fe and paramagnetic Pt were first performed to establish the intrinsic electronic structures of the pure elements before introducing alloying effects. The calculated band structures confirm the metallic nature of both Fe and Pt. From the DOS demonstrates that d-electrons dominate the electronic behavior of Fe and Pt. Systematic DOS calculations using the TB-LMTO and Haydock recursion schemes provide insight into SOC effects in the Fe-Pt system. The DOS comparison of ordered $FePt_3$, FePt, and Fe_3Pt indicates that SOC significantly alters the electronic structure, and that the extent of these alterations increases with Pt concentration. The rightward displacement of one spin component and the leftward displacement of the other suggest that SOC leads to variations in spin polarization, consequently altering magnetic moment. This effect is most pronounced in Pt-rich alloys owing to the stronger SOC characteristic of heavier elements such as Pt.

The computed data and graphical results show that the inclusion of SOC leads to a sharp increase in band energy and magnetic moment. The observed variation in band energy with and without SOC indicates that higher Pt concentrations enhence SOC effects, leading to greater changes in the band structure and an increase in the magnetic moment. The increase in magnetic moment with increasing Pt concentration under SOC conditions highlights the role of spin polarization and hybridization effects in determining the magnetic properties of the alloy. For disordered Fe_xPt_{1-x} alloys, the spin-orbit coupling parameters were obtained from interpolation equations and utilized in the TB-LMTO calculations. These parameters were validated through close consistency with available data. The calculated density of states for various compositions also confirms that SOC reduces the overlap between spin-up and spin-down DOS, thereby enhancing spin polarization. The observed trend in band energy for disordered alloys supports the conclusion that SOC effects become more pronounced with increasing Pt concentration. The study further demonstrates the effectiveness of employing the recursion method in modeling the complex SOC effects on the electronic and magnetic properties of FePt alloys. The results are consistent with predictions from theoretical calculations and previously published works, thereby validating the suitability of the computational method employed in this work. The magnetic moment and band energy increase upon incorporating SOC, highlighting its critical role in defining the electronic and magnetic properties of Fe-Pt alloys. Overall, the findings highlight the importance of spin-orbit coupling in modulating the electronic and magnetic properties of Fe-Pt alloys, particularly in Pt-rich compositions. The study illuminates the interplay between SOC, electronic structure, and magnetism, and paves the way for further exploration of spin-dependent phenomena in transition metal alloys. Future work could focus on extending these investigations to include temperature-dependent effects and on the experimental confirmation of theoretical calculations to further enhance the understanding of SOC in complex alloy systems.

ACKNOWLEDGEMENTS

This work is funded by a research grant provided by the University Grants Commission through the authority of Jagannath University.

REFERENCES

[1] K. M. Krishnan, A. B. Pakhomov, Y. Bao, P. Blomqvist, Y. Chun, M. Gonzales, K. Griffin, X. Ji and B. Roberts, Nanomagnetism and spin electronics: materials, microstructure and novel properties, *J. Mater. Sci.* **41**,793–815, 2006.

[2] K. M. Krishnan, C. Nelson, C. J. Echer, F. R. C. Farrow, R. F. Marks, A. J. Kellock, "Exchange biasing of permalloy films by Mn_xPt_{1-x}: role of composition and microstructure", *J. Appl. Phys*. **83** (11), 6810–6812, 1998.

[3] T.A.P. Rocha-santos, Trends in Analytical Chemistry Sensors and biosensors based on magnetic nanoparticles, *Trends Anal. Chem.* **62**, 28–36, 2014.

[4] M. Futamoto, M. Nakamura, M. Ohtake, Growth of L1 0 -ordered crystal in FePt and FePd thin films on MgO (001) substrate, 085302, 2016.

[5] K. M. Krishnan, C. Nelson, C. J. Echer, R. F. C. Farrow, R. F. Marks, A. J. Kellock, K .M. Krishnan, C. Nelson, C.J. Echer, Exchange biasing of permalloy films by Mn x Pt 1 − x : Role of composition and microstructure Exchange biasing of permalloy films by Mn x Pt 1 ⁄ x : *Role of composition and*

microstructure, 6810, 21–24, 2014.

[6] S. C. Tsang, C. H. Yu, H. Tang, H. He, V. Castelletto, I. W. Hamley, T. Narayanan, C. C. H. Lo, K. Tam, Assembly of Centimeter Long Silica Coated FePt Colloid Crystals with Tailored Interstices by Magnetic Crystallization, 4554–4556, 2008.

[7] T. S. Rodrigues, A. G. M. da Silva, P. H. C. Camargo," Nano-catalysis by noble metal nanoparticles: controlled synthesis for the optimization and understanding of activities", *J. Mater. Chem.* **7** (11), 5857–5874, 2019

[8] Soven, Paul, "Coherent-Potential Model of Substitutional Disordered Alloys". *Physical Review.* **156** (3): 809–813, 1967.

[9] K. Hohenberg, Pierre; Walter, "Inhomogeneous electron gas". *136* (3B): B864–B871, *Phys. Rev.* B. 136, B864–B871, 1964.

[10] A. Mookerjee, A new formalism for the study of configuration averaged properties of disordered systems, *J. Phys. C Solid State Phys.* **6**, 1973.

[11] H. Search, C. Journals, A. Contact, M. Iopscience, Electronic structure based on the local atomic environment for tight-binding bands, 2845, 1972.

[12] R. Haydock and M. J. Kelly, 'Surface densities of states in the tight-binding approximation', *Surf. Sci.* **38**, 139, 1973.

[13] A. Huda, D. Paudyal, A. Mookerjee, M. Ahmed, Spin-orbit coupling : A recursion method approach, *Phys. B: Cond. Mat.*, **351**, 63–70, 2004.

[14] N. U. Luchini, C. M. M. Nex, 'A new procedure for appending terminators in the recursion method', *J Phys. C: Solid State Phys.*, **20**, 3125, 1987.